


Article

Design and Optimization of a Compact Ultra-Broadband Polarization Beam Splitter for the SCL-Band Based on a Thick Silicon Nitride Platform

Georgios Patsamanis ^{1,2,*} , Dimitra Ketzaki ^{1,3}, Dimitrios Chatzitheocharis ^{1,2} and Konstantinos Vyrsokinos ^{1,2}

¹ Centre for Interdisciplinary Research and Innovation, Aristotle University of Thessaloniki, 57001 Thessaloniki, Greece

² School of Physics, Aristotle University of Thessaloniki, 54124 Thessaloniki, Greece

³ Department of Informatics, Aristotle University of Thessaloniki, 54124 Thessaloniki, Greece

* Correspondence: gpatsama@auth.gr; Tel.: +30-697-914-5250

Abstract: The polarization beam splitter is an essential photonic integrated circuit in applications where a high-performing on-chip polarization diversity scheme is required. The lower refractive index contrast of the silicon nitride material platform compared to silicon-on-insulator constitutes the separation of polarized light states a challenging task since for this purpose a large difference between the effective refractive indices of the fundamental TE and TM modes is highly desirable. In this paper, we present the design and optimization analysis of an ultra-broadband polarization beam splitter based on a thick silicon nitride platform through extensive 3D-FDTD simulations. The proposed device exploits two different Si₃N₄ thicknesses that enable the discrimination of the two polarizations at the proximity of an 800 nm thick slot and a 470 nm thick strip waveguide via directional coupling. The proposed two-stage PBS achieves higher than 30.6 dB polarization extinction ratio (PER) for both TE and TM polarizations across a 130 nm span at the SCL-band. The dimensions of the PBS are 94 × 14 μm² and the insertion losses are calculated to be lower than 0.8 dB for both polarizations. The fabrication tolerance of the device is also discussed.

Keywords: polarization beam splitter; silicon nitride; directional coupling; 3D-FDTD method



Citation: Patsamanis, G.; Ketzaki, D.; Chatzitheocharis, D.; Vyrsokinos, K. Design and Optimization of a Compact Ultra-Broadband Polarization Beam Splitter for the SCL-Band Based on a Thick Silicon Nitride Platform. *Photonics* **2022**, *9*, 552. <https://doi.org/10.3390/photonics9080552>

Received: 6 July 2022

Accepted: 4 August 2022

Published: 6 August 2022

Publisher's Note: MDPI stays neutral with regard to jurisdictional claims in published maps and institutional affiliations.



Copyright: © 2022 by the authors. Licensee MDPI, Basel, Switzerland. This article is an open access article distributed under the terms and conditions of the Creative Commons Attribution (CC BY) license (<https://creativecommons.org/licenses/by/4.0/>).

1. Introduction

Silicon photonics keeps reporting a remarkable progress on the design and manufacturing of compact and efficient photonic integrated circuits (PICs), paving the way for densely packaged photonic systems combining high-speed operation, low power consumption and cost [1,2]. Both silicon-on-insulator (SOI) and silicon nitride (Si₃N₄) CMOS-compatible integration platforms address the needs for PICs operating in the near and mid-IR regime for a wide range of applications such as telecommunications, optical signal processing, lidar and sensing [3–5]. The functionality of PICs can be significantly enhanced via polarization management and as such Polarization Beam Splitters (PBSs) are vital components towards this direction, as they enable applications requiring polarization-division multiplexing [6,7]. The high refractive index contrast of SOI ($\Delta n \approx 2.0$ at 1.55 μm) has led to a maturity and miniaturization of broadband PBS devices with remarkable performance [8,9]. The Si₃N₄ platform, on the other hand, exhibiting lower index contrast ($\Delta n \approx 0.52$ at 1.55 μm) demands sophisticated approaches in terms of PIC design for the separation of the TE and TM modes. So far, a plethora of Si₃N₄-based PBSs have been demonstrated relying on different polarization handling mechanisms such as phase-controlled directional couplers (DC) [10–12], slot-based DCs [13], multimode interference (MMI) and angled MMI couplers [14,15], cascaded asymmetric DCs [16] and 3D DCs [17]. Although these PBSs take advantage of such well-established polarization splitting techniques, an all-inclusive design for Si₃N₄ featuring very high performance in terms of minimum polarization extinction

ratio (PER) across a large wavelength range (>100 nm), low insertion losses (IL) and small footprint is yet to be reported. The above performance metrics are even harder to achieve in Si_3N_4 waveguides of more than 600 nm thickness, where the effective refractive indices are almost identical for the TE and TM polarizations. Si_3N_4 waveguide technology with thickness between 600 nm and 800 nm offers high mode confinement that facilitates frequency comp generation [18], quantum optics [19], optical phased arrays [20], as well as coupling with InP lasers [21], and deploying a high-performing Si_3N_4 PBS on the same layer thickness would offer remarkable benefits in terms of polarization management.

In this work, we present the design and optimization analysis of an ultra-broadband and compact Si_3N_4 PBS design that relies on an 800 nm thick slot waveguide and a 470 nm strip waveguide, exploiting the directional coupling scheme and operating in the SCL-band. The structure of the paper is as follows: Section 2 presents the design of a single vertical-slot-based PBS and explains the principle of operation. At this stage, the PBS design is optimized at 1550 nm wavelength, featuring a minimum PER of 13.8 dB across the 1500–1630 nm range for both TE and TM polarizations. Section 3 presents the optimization analysis that is targeting to enhance the minimum PER by maximizing performance at two different wavelengths and applying then a two-stage cascaded formation. The three-dimensional finite-difference time-domain (3D-FDTD) analysis shows then a maximum PER and IL of 30.6 dB and 0.8 dB, respectively, for both TE and TM polarizations with a footprint of only $94 \times 14 \mu\text{m}^2$ across the same SCL-band. Section 4 discusses the tolerance to fabrication errors, when two critical parameters; the thickness of the waveguides and the gap in the DC section deviate independently and simultaneously from their optimized values by $\Delta t/h = \pm 16$ nm and $\Delta G = \pm 20$ nm, respectively, resulting to a minimum PER of 22.8 dB in the worst-case scenario that confirms the resilience of the proposed PIC layout. Finally, in Section 5 the proposed PBS design is compared with various state-of-the-art Si_3N_4 counterparts, and the paper concludes summarizing the key results.

2. Design and Principle of Operation

The proposed all silicon nitride-based PBS consist of an 800 nm thick and 800 nm fixed width vertical slot waveguide with a gap g , and a strip waveguide of thickness t and 800 nm width, as illustrated in the schematic of Figure 1. The TE/TM polarized input light enters the device from the strip waveguide and is split to the two output strip waveguides with different heights. The two types of waveguides support only the fundamental modes, and the polarization selectivity is achieved by ensuring the phase-matching condition for the TM_0 mode that is directionally coupled to the slot waveguide and exits the device from the cross port. The TE mode remains at the strip waveguide and exits the device from the through port. The light is exchanged between the two types of waveguides in the coupling section of length L_c , featuring a gap, G . An S-bend is used for the separation of the two ports, with a radius of 50 μm aiming to avoid the induction of any polarization rotation of the fundamental modes, or additional propagation losses. The refractive index n of the Si_3N_4 waveguides at 1550 nm wavelength is taken as 1.974 and of the surrounding SiO_2 cladding as 1.45.

Figure 1b shows the cross-sectional geometry of the two types of waveguides in the coupling region of the DC-based PBS with all fixed values and the parameters under investigation. The supported TE and TM modes of the strip and slot waveguides that eventually propagate to the through and cross ports, respectively, are visualized in Figure 1c. The gap of the slot waveguide is linearly decreased to 150 nm after the coupling region in order to ensure almost lossless transition of the propagating TM mode from the slot to a square $800 \times 800 \text{ nm}^2$ waveguide, complying simultaneously with the 193 nm DUV lithography limits.

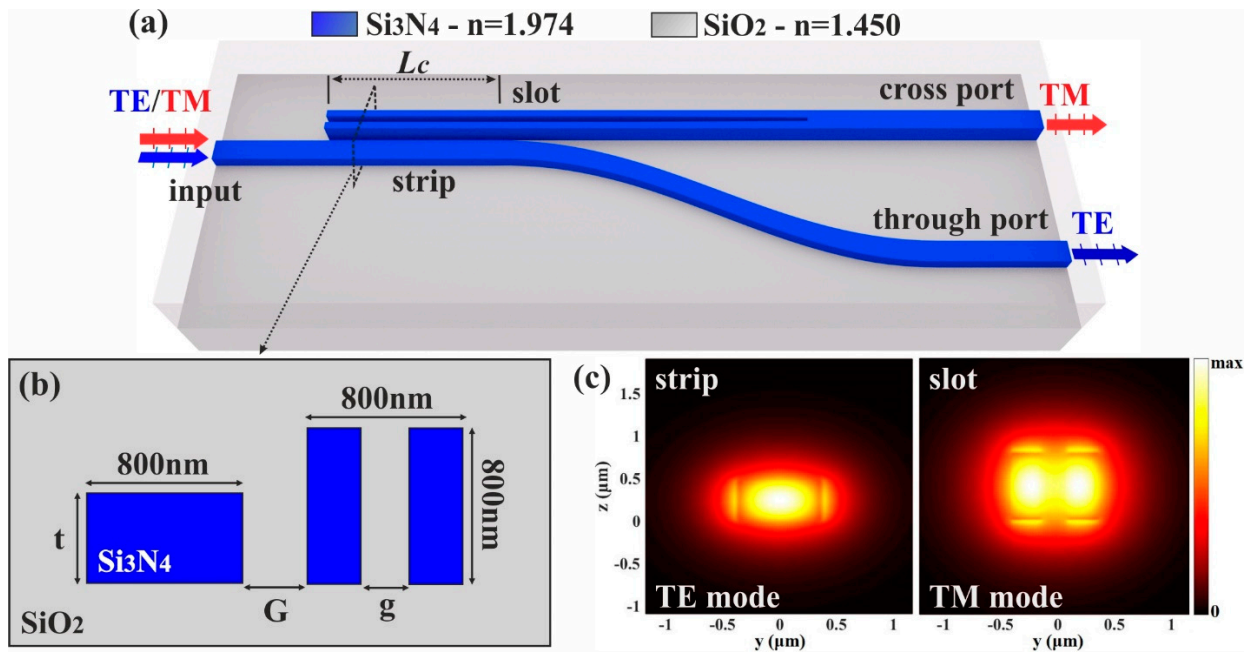


Figure 1. (a) Illustration of the proposed DC-based PBS layout consisting of the strip and slot waveguides. The blue arrow represents the TE polarization, and the red arrow the TM. (b) Cross sectional view of the waveguides in coupling region where polarization discrimination is achieved. (c) Modal profiles of the supported TE and TM modes in the strip and waveguide, respectively.

Optimization of the DC-Based PBS for 1550 nm Wavelength

According to the coupled mode theory (CMT) [22], to achieve the phase-matching condition for efficiently coupling evanescently the TM polarized light to the vertical slot waveguide in Figure 1a, the following condition $\Delta n_{\text{eff}}^{\text{TM}} = n_{\text{eff}}^{\text{TMstrip}} - n_{\text{eff}}^{\text{TMslot}} = 0$ should be fulfilled by applying the proper combination of design parameters, i.e., g and t , to the two waveguides. On the contrary, the phase-mismatch of the TE polarization can be secured when the highest possible difference between the TE mode effective indices of the strip and slot waveguide, $\Delta n_{\text{eff}}^{\text{TE}} = n_{\text{eff}}^{\text{TEstrip}} - n_{\text{eff}}^{\text{TEslot}}$, is obtained. In this way, the TM polarized light will be coupled with maximum efficiency to the through port, while the TE polarized light will remain uncoupled to the strip waveguide. These conditions are considered quite challenging to meet for the thick (>600 nm) Si_3N_4 material platform that exhibits (i) a medium refractive index contrast of $\Delta n \approx 0.5$ and ii) close to rectangular waveguide cross sections in contrast to thin (<150 nm) platforms that usually feature an aspect ratio higher than six [23].

The design optimization of the PBS device starts with the calculations of the fundamental TE and TM modes in the slot and strip waveguides for 1550 nm wavelength, by applying the finite-difference eigenmode calculation (FDE) method on the varying cross-sectional geometry. Figure 2a,b shows the calculated effective refractive indices of the TE (blue line) and TM (red line) modes for the slot waveguide with $G = 300$ nm and varying g , and for the strip waveguide with varying t , along with the respective effective refractive index difference of the modes, Δn_{eff} (TM-TE) (purple dashed line), in each case.

According to the results of Figure 2, the mode phase-matching of TM occurs for the combination of $g = 250$ nm and $t = 470$ nm, and the effective refractive index of the TM polarization in each waveguide is 1.579, as noted by the horizontal red dotted lines. In addition, the $\Delta n_{\text{eff}}^{\text{TE}}$ value is estimated to 0.086 for these optimum design parameters and can ensure the TE polarized light will propagate to a large degree in the strip waveguide. The Δn_{eff} (TM – TE) curves indicate that the highest $\Delta n_{\text{eff}}^{\text{TE}}$ value of 0.094 is obtained for $g = 245$ nm and $t = 360$ nm, but in this case the $\Delta n_{\text{eff}}^{\text{TM}}$ would be only 0.07.

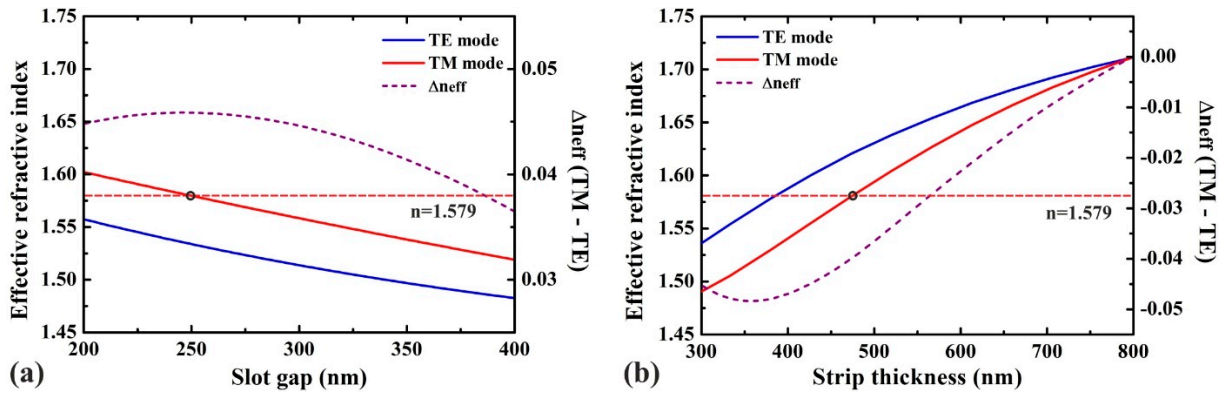


Figure 2. Calculated effective refractive indices of the TE and TM modes and the respective Δn_{eff} at 1550 nm for the (a) slot waveguide with varying g and the (b) strip waveguide with varying t .

Having specified the proper waveguide geometries, for maximum coupling of the TM mode to the cross port, the design methodology now focuses on calculating the optimum length of the coupling section of the PBS at the coupled waveguide system. The length of parallel waveguides that is required for completely transferring the TM polarization from one waveguide to another is expressed by the beat length L_{π} [24]:

$$L_{\pi} = \frac{\lambda}{2(n_{\text{eff0}}^{\text{TM}} - n_{\text{eff1}}^{\text{TM}})} \tag{1}$$

where $\lambda = 1550$ nm the central wavelength of operation, and $n_{\text{eff0}}^{\text{TM}}$ and $n_{\text{eff1}}^{\text{TM}}$ the effective indices of the fundamental (even) and first order (odd) TM modes of the coupled waveguide system in the coupling section, respectively. By applying $g = 250$ nm and $t = 470$ nm, where $\Delta n_{\text{eff}}^{\text{TM}} = 0$ and $\Delta n_{\text{eff}}^{\text{TE}} = 0.086$ as noted, a beating length of $L_{\pi} = 15.15 \mu\text{m}$ is calculated. However, by taking into account the contribution of the S-bend to the light coupling, the actual length L_c will have a lower value than L_{π} , that is calculated by a series of 3D-FDTD simulations across the entire structure under investigation. Figure 3a shows the transmission of the TM mode to the cross and through port with varying L_c at 1550 nm wavelength. As expected, the coupling efficiency of the TM mode to the slot waveguide presents a maximum at -0.18 dB around an L_c value of $10.3 \mu\text{m}$, while the transmission to the through port has a minimum value of -27.3 dB for this wavelength. The next step is the calculation of the wideband transmission of the TE and TM modes for $L_c = 10.3 \mu\text{m}$ across the 1500–1630 nm wavelength range with corresponding results depicted in Figure 3b. For the TE polarization, the transmission loss to the through port remains above -0.2 dB and to the cross port ranges between -14.2 dB to -18.7 dB. For the TM polarization, the transmission loss to the through port ranges between -15.8 dB and -27.4 dB, while the cross port is above -0.23 dB for the entire span under investigation.

The performance metric of the PBS is evaluated by calculating the polarization extinction ratio (PER) of both polarizations at the corresponding output ports. The PER value is extracted from the equations:

$$\text{PER}_{\text{TE}} = T_{\text{TE}}^{\text{through}} - T_{\text{TM}}^{\text{through}}, \tag{2}$$

$$\text{PER}_{\text{TM}} = T_{\text{TE}}^{\text{cross}} - T_{\text{TM}}^{\text{cross}} \tag{3}$$

where, $T_{\text{TE}}^{\text{through}}$, $T_{\text{TM}}^{\text{through}}$, $T_{\text{TE}}^{\text{cross}}$ and $T_{\text{TM}}^{\text{cross}}$ are the transmitted power of the TE and TM modes expressed in dB at the through and cross ports, respectively, as illustrated in Figure 3b. The PER_{TE} corresponds to the purity of the dominant TE polarization at the through port, while the PER_{TM} to the purity of the dominant TM polarization at the cross port. Figure 3c presents the calculated broadband PER of both polarizations across the investigated 130 nm wavelength span, revealing a minimum value of 15.6 dB for PER_{TE} and 13.8 dB for PER_{TM} .

The same figure shows a strong dependency of the PER_{TE} that was expected since the polarization discrimination relies on the wavelength dependent DC mechanism. Regarding the maximum values, the phase-matching and mismatching conditions allow the proposed layout to reach PER_{TE} and PER_{TM} values up to 27.3 dB and 18.5 dB, respectively. In addition, Figure 3d,e illustrate for the proposed optimum conditions the electric field distributions of TE and TM at 1550 nm where the dominant field components are the E_y and E_z , respectively. The IL for this part of the device ranges between 0.04 dB and 0.07 dB for the TE polarization across the whole band and between 0.16 dB and 0.18 dB for the TM polarization, with the extra ~0.1 dB mainly associated to the transition via the slot taper. The total length of the PBS design is 36.5 μm , the total width is 6 μm and the gap between the output ports is 4.4 μm .

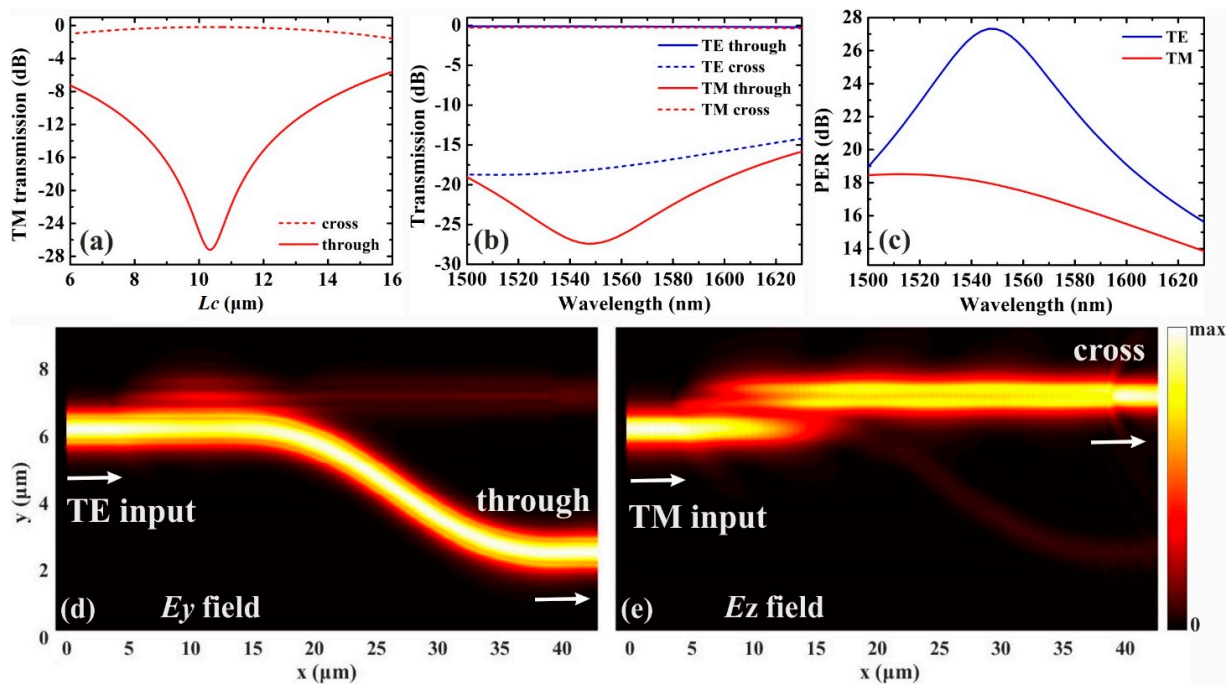


Figure 3. (a) Calculated transmission of the TM mode versus L_c . (b) TE and TM mode wideband transmission for $L_c = 10.3 \mu\text{m}$. (c) Device PER for TE and TM polarization. Electric field distribution along the PBS for (d) TE and (e) TM input polarizations.

3. Cascaded Formation for Enhanced Performance at Wide Wavelength Range

3.1. Variation of L_c and G

The ultra-small size of the proposed PBS grants the opportunity for the investigation of a cascaded layout, aiming towards an ultrahigh broadband performance in terms of PER_{TE} and PER_{TM} , while still maintaining a very low total device footprint. This tailor made performance can be obtained by varying the parameter L_c from 9 to 11.5 μm that adjusts the minimum PER_{TE} and PER_{TM} at the edges of the targeted wavelength span. The combination thus of cascaded PBSs with different L_c provides a device with enhanced performance across the targeted 1500–1630 nm range.

Figure 4 shows the calculated PER over the 1500–1630 nm wavelength range for both polarizations versus the L_c . The TE polarization according to Figure 4a, exhibits PER_{TE} more than 18.8 dB at 1500 nm for $L_c > 11 \mu\text{m}$, and more than 22.9 dB at 1630 nm for $L_c < 9.5 \mu\text{m}$. The very high values of PER_{TE} observed around 1580 nm indicate that strong phase-matching in the proposed DC-based PBS also occurs for this wavelength region. The performance for the TM polarization is illustrated in Figure 4b and the PER_{TM} exhibits more than 15.3 dB across the whole wavelength span for $L_c = 11.5 \mu\text{m}$, while the minimum value is 10.5 dB for $L_c = 9 \mu\text{m}$ at 1630 nm. Overall, the variation of L_c leads to a change in the spectral position of the PER_{TE} peak, while for PER_{TM} the preference is for larger L_c

where the minimum value increases. A proper combination thus of these two layouts could deliver the desired broadband performance in terms of PER for both polarizations. The next optimization stage is the investigation of the spectral response for these two L_c , by varying the design parameter G . Figure 5 shows the calculated PER_{TE} and PER_{TM} for L_{c1} and L_{c2} when G varies between 280 nm–320 nm. According to what is expected, the variation of G leads in a change of the position of the peak of PER_{TE} and of the minimum values of PER_{TM} . Figure 5a reveals that for $L_{c1} = 9 \mu\text{m}$, PER_{TE} is calculated to be everywhere higher than 15 dB with maximum values reached at 1580 nm for $G \sim 285 \text{ nm}$. Also, according to Figure 5b, PER_{TM} is higher than 11 dB for $G < 285 \text{ nm}$. On the other hand, from Figure 5c for $L_{c2} = 11.5 \mu\text{m}$, PER_{TE} is everywhere higher than 14 dB for $G > 315 \text{ nm}$, with maximum values obtained at 1545 nm. Finally, from Figure 5d the minimum PER_{TM} is higher than 15.5 dB for $G > 315 \text{ nm}$. Therefore, choosing a PBS with L_{c1} and $G < 285 \text{ nm}$ can increase the minimum values for both PER_{TE} and PER_{TM} and move the peak of PER_{TE} closer to 1580 nm, while choosing L_{c2} with $G > 315 \text{ nm}$ can further boost minimum PER_{TM} and move PER_{TE} closer to 1545 nm. The 3D-FDTD simulations reveal also that the IL remain below 0.23 dB for all L_c and G combinations.

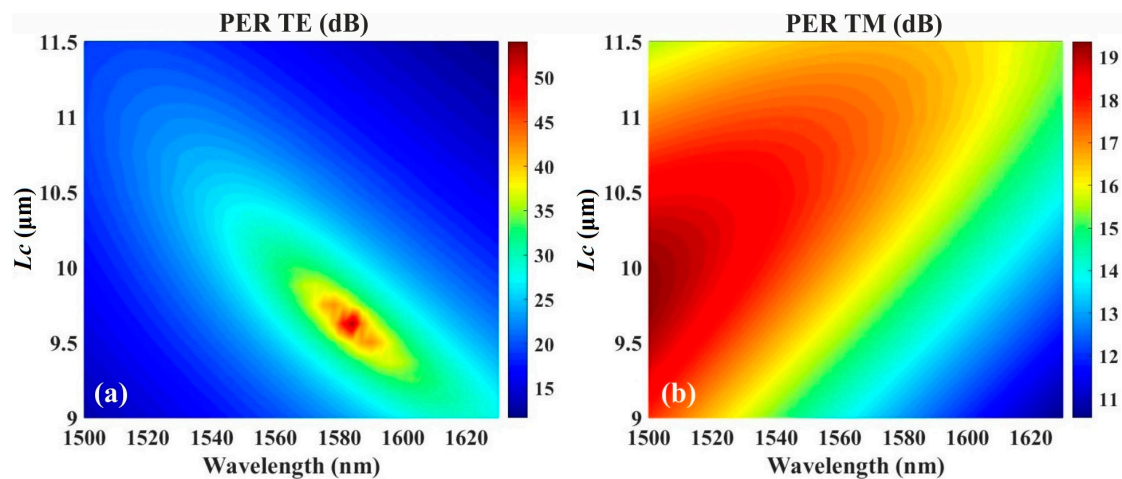


Figure 4. Calculated PER of the (a) TE and (b) TM polarization when L_c varies between 9–11.5 μm .

3.2. Cascaded Formation

Having calculated the broadband performance of a single PBS by varying the two major design parameters L_c and G , we proceed to the design and analysis of the two-stage cascaded formation targeting to maximize the PER values across the entire 1500–1630 nm band, at the expense of total dimensions and insertion losses. Figure 6 illustrates the proposed layout where three DCs with different combinations of selected L_c and G are employed. The input light is injected into the PBS from the 470 nm thick strip waveguide to DC1, where the cross/through ports are connected to DC2/DC3, respectively. The transition from DC1 to DC2, as shown in the left inset of Figure 6, is carried out via a 10 μm long rib-type taper with a tip of 150 nm that adiabatically transfers the light from the 800 nm to the 470 nm thick waveguide. The TM polarized light is monitored from the cross port of DC2 referred as port 1, while the TE lightwave is recorded from the through port of DC3, marked as port 4. The through port of DC2 and the cross port of DC3, labeled as port 3 and port 4, respectively, collect the residual unwanted TE and TM light for subsequent suppression of any unwanted back reflections via taper tips. The right inset of Figure 6 shows details about this part of the PBS layout.

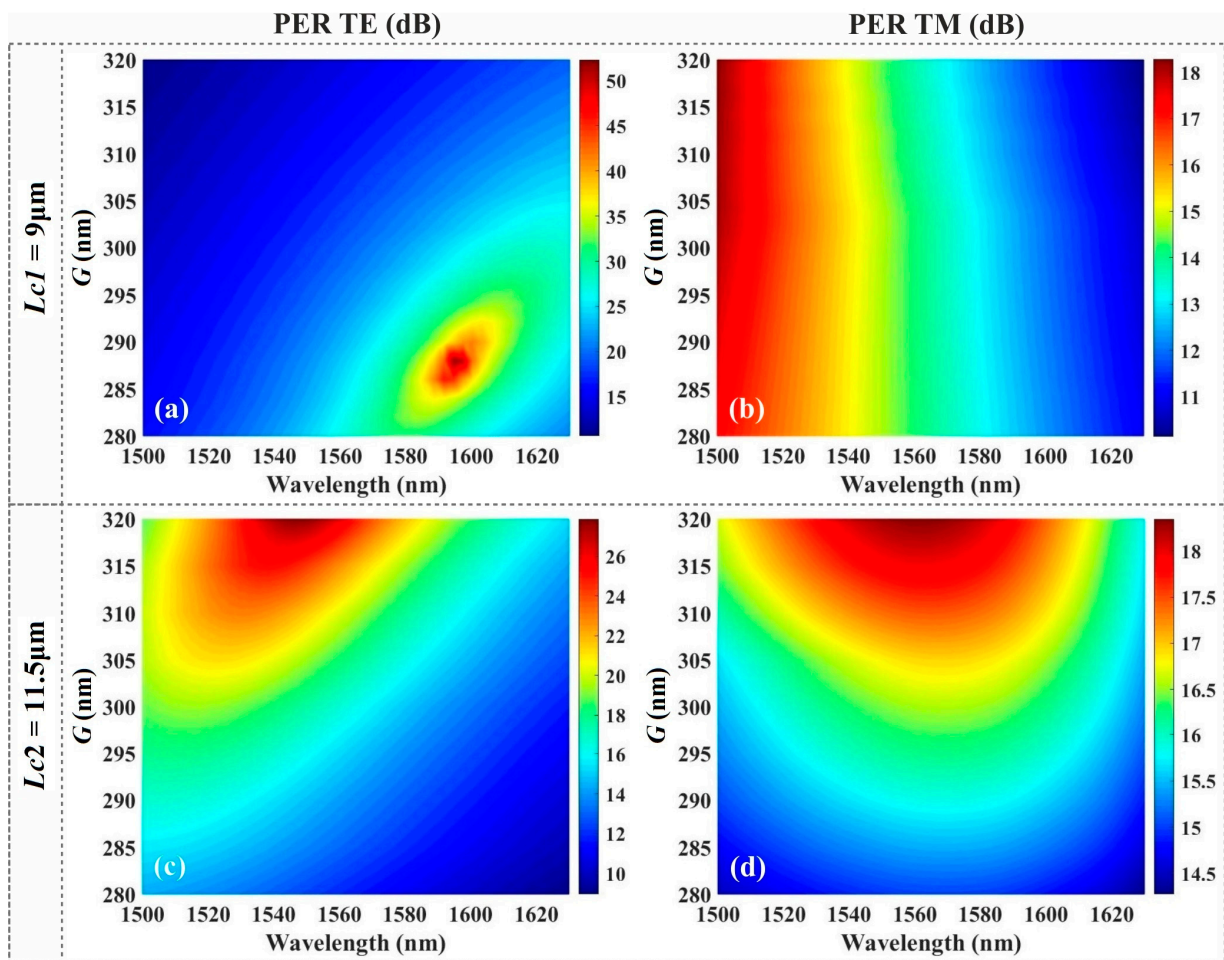


Figure 5. Calculated TE and TM PER when G varies between 280 nm and 320 nm for (a,b) $L_{c1} = 9 \mu\text{m}$ and (c,d) $L_{c2} = 11.5 \mu\text{m}$, respectively.

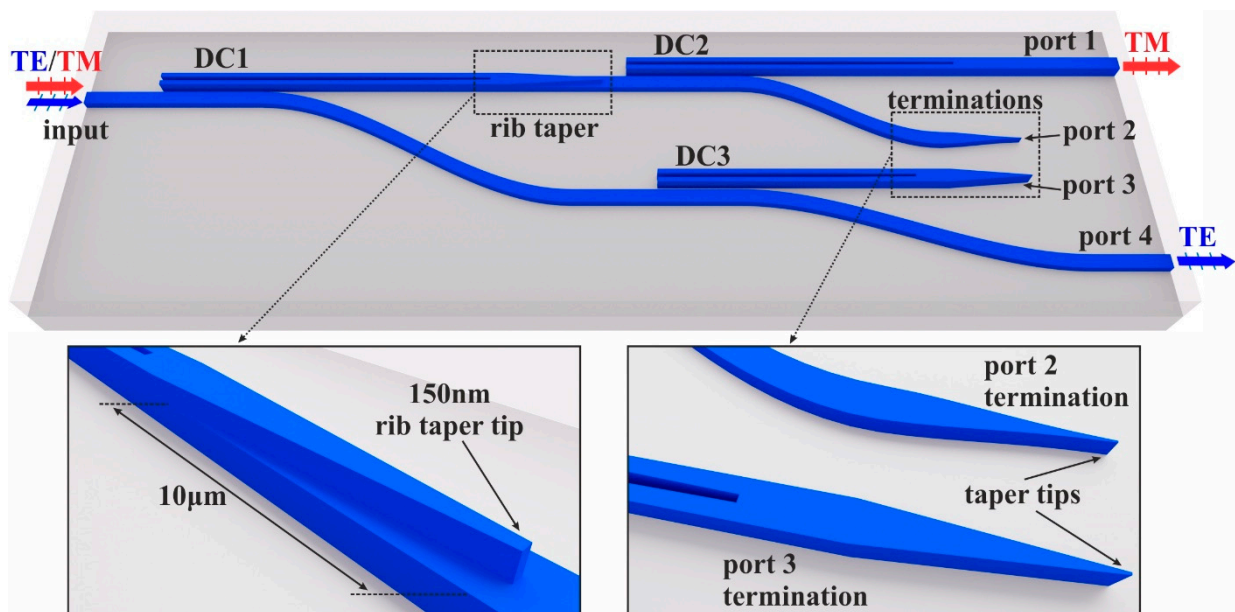


Figure 6. Two-stage cascaded formation employing three PBSs, DC1, DC2 and DC3 with selected L_c and G . An adiabatic rib taper is used for the transition from DC1 and DC2 and the ports that are not used as outputs are terminated, as shown in the insets.

The optimum PBS design is coming from a combination featuring identical DC1 and DC2 with $L_{c2} = 11.5 \mu\text{m}$ and $G = 320 \text{ nm}$, while for DC3 the corresponding key parameters are $L_{c1} = 9 \mu\text{m}$ and $G = 280 \text{ nm}$. Figure 7a shows the DC1 & DC2 transmission curves for TE/TM polarization and Figure 7b for DC3, both extracted by 3D-FDTD simulations. The two graphs reveal that the IL are below 0.22 dB for DC1 & DC2 and less than 0.23 dB for DC3 with a flat response. Also, from the same graphs it is shown that the minimum PER_{TE} for DC3 is located at 1500 nm with a value of 16.4 dB, while the minimum PER_{TM} is of 10.9 dB at 1630 nm. On the other hand, DC1 & DC2 presents a symmetric performance with a minimum PER_{TE} , PER_{TM} of 15 dB and 15.5 dB respectively, both at 1630 nm. Figure 7c illustrates the calculated aggregated transmission curves of the cascaded DC scheme, extracted from transfer matrix simulations, taking into account the S-parameters of DC1/DC2 and of DC3 from Figure 7a,b. The transfer matrix method was selected at this point, eliminating the need to simulate the entire device with 3D-FDTD that would require enormous computational resources. It should be pointed out that the model also considers in the transfer matrix the IL of the rib taper for the transition between the two different thicknesses that is less than 0.06 dB. This advanced PBS scheme now induces IL in the range of 0.23–0.57 dB for TE light and between 0.48 dB and 0.8 dB for TM polarization in the entire 130 nm window. Figure 7d displays the performance in terms of PER, revealing minimum values of 34.3 dB and 30.6 dB for PER_{TE} and PER_{TM} respectively, granting the ultra-high polarization selectivity in combination with ultra-broadband performance targeted at the start of this work. It should be noted that these high PER values allow high margin for error during fabrication as it will be shown in the next Section.

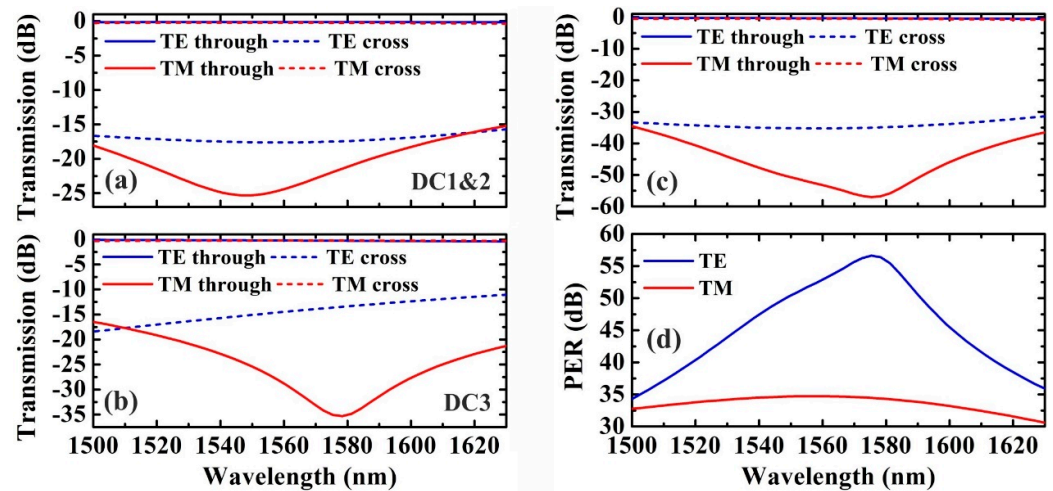


Figure 7. Calculated PER for TE and TM polarization of the (a) DC1 & DC2 and (b) DC3 devices. (c) Aggregated transmission and (d) PER at the TE and TM ports of the two-stage cascaded formation.

The total dimensions of the proposed formation are estimated at $94 \times 14 \mu\text{m}^2$ by 2D-layouting and the gap between the output ports 1 and 4 is $12.4 \mu\text{m}$. It is worth noting that when deploying the specific DCs of Figure 7, the minimum PER of the device is improved by 3.3 dB and 3 dB for TE and TM polarization, respectively, compared to the layout that employs three identical PBSs of Figure 3c optimized for 1550 nm. In addition, the IL for the TM port can be further reduced by narrowing the tip of the slot tapers down to 50 nm, reaching overall values lower than 0.4 dB. On the other hand, when the width of the slot tip is 250 nm instead of 150 nm, the IL is raised up to 1.4 dB for TM polarization. For the TE light the corresponding values are 0.5 dB for 50 nm and 0.9 dB for 250 nm slot gap. Table 1 summarizes the design parameters of the PBSs in the proposed cascaded scheme and their performance across the 1500–1630 nm wavelength range.

Table 1. Design parameters of the two DCs.

PBS	L_c (μm)	G (nm)	PER_{TE} (dB)	PER_{TM} (dB)	IL (dB)
Single DC1/DC2	11.5	320	>15	>15.3	<0.23
Single DC3	9	280	>16.3	>10.7	<0.22
Cascaded			>34.3	>30.6	<0.80

4. Fabrication Tolerance Analysis

Taking into consideration that DCs are very sensitive to fabrication variations, it is important to evaluate numerically the impact of deviations from the optimum geometry to the overall performance of the device. The fabrication tolerance is initially investigated by simultaneously varying the thickness of both types of waveguides, Δth , for DC1/DC2 and DC3 by ± 16 nm with a step of ± 2 nm. The next step is to change the gap G by ± 20 nm for $\Delta th = \pm 16$ nm, so as to identify which parameters affects mostly the PER of the proposed PBS. The other crucial parameter for the DC mechanism that is the form (gap, sidewalls) of the slot waveguide is not considered a variable for this tolerance analysis, as for a complete investigation three different parameters should be varied: the gap g and the width of two side walls, where their interplay affects the total width and form of the slot waveguide, rendering this task extremely complex.

The effect of the simultaneous variation of thickness, Δth , at both types of waveguides on PER_{TE} and PER_{TM} for a single DC is depicted in Figure 8. According to Figure 8a,b for DC1/DC2, minimum PER_{TE} ranges between 12.3 dB and 12.7 dB at the edges of the wavelength range, while minimum PER_{TM} is between 13.4 dB and 14.9 dB. Also Figure 8c,d shows that for DC3 the minimum PER_{TE} ranges between 12.8 dB and 16.5 dB at the edges of the wavelength range, while the minimum PER_{TM} is between 9.5 dB and 12.4 dB. Overall, it is clear and in agreement from what was expected that deviations in thicknesses will result to a decline in efficiency of the DCs for TE or TM polarization, or both, therefore affecting the performance of the overall device.

Having calculated the performance degradation of the two DCs versus the variation of Δth , the next step is to proceed to the extraction of the worst-case scenario when G also deviates from its optimal value by ± 20 nm with corresponding results presented in Figure 9. Figure 9a reveals that the deviation of the thicknesses by -16 nm or $+16$ nm leads to a minimum PER_{TE} of 32.4 dB or 26.8 dB, respectively, while according to Figure 9b the PER_{TM} minimum value is 23 dB for Δth of -16 nm and 28.9 dB for Δth $+16$ nm at the upper end of 1630 nm. Going now to the worst-case scenario where the gap G deviates also from its optimum value for $\Delta th = \pm 16$ nm, Figure 9c shows that minimum PER_{TE} lies between 28.9 dB and 22 dB for all combinations with the worst one emerging for $\Delta th = +16$ nm and $\Delta G = +20$ nm. From Figure 9d it is also evident that for TM polarization, minimum PER_{TM} is 22.6 dB for the combination of $\Delta th = -16$ nm and $\Delta G = +20$ nm with a clear trend for lower values as the operation wavelength increases. The comparison between Figure 9a,c and Figure 9b,d reveals that precise control of Δth is crucial in order to maintain very good wideband PER performance, especially for TM polarization. On the other hand, ΔG seems to have minor effect in the overall performance of the cascaded layout. Regarding the degradation of the IL from fabrication errors, according to Figure 9e,f TE light features a maximum value of ~ 1.2 dB for the worst case of $\Delta th = -16$ nm and $\Delta G = +20$ nm, while TM does not exceed 1.1 dB, when $\Delta th = -16$ nm and $\Delta G = -20$ nm, respectively. Comparing these results with the optimum design presented in Section 3, the minimum PER_{TE} declines up to 12.3 dB and the PER_{TM} up to 8 dB for these assumed worst-case scenarios, where both Δth and ΔG values are missed by the widest accepted margin in lithography, deposition and etching of the Si_3N_4 core layer. It should be noted that if a PER of 20 dB is considered acceptable, the proposed design has a 2 dB margin for even higher tolerance to fabrication errors. Also, if a maximum 1.5 dB theoretical value is considered acceptable for the IL, there is still space for relaxing even further the fabrication tightness coming with the DC sensitivity.

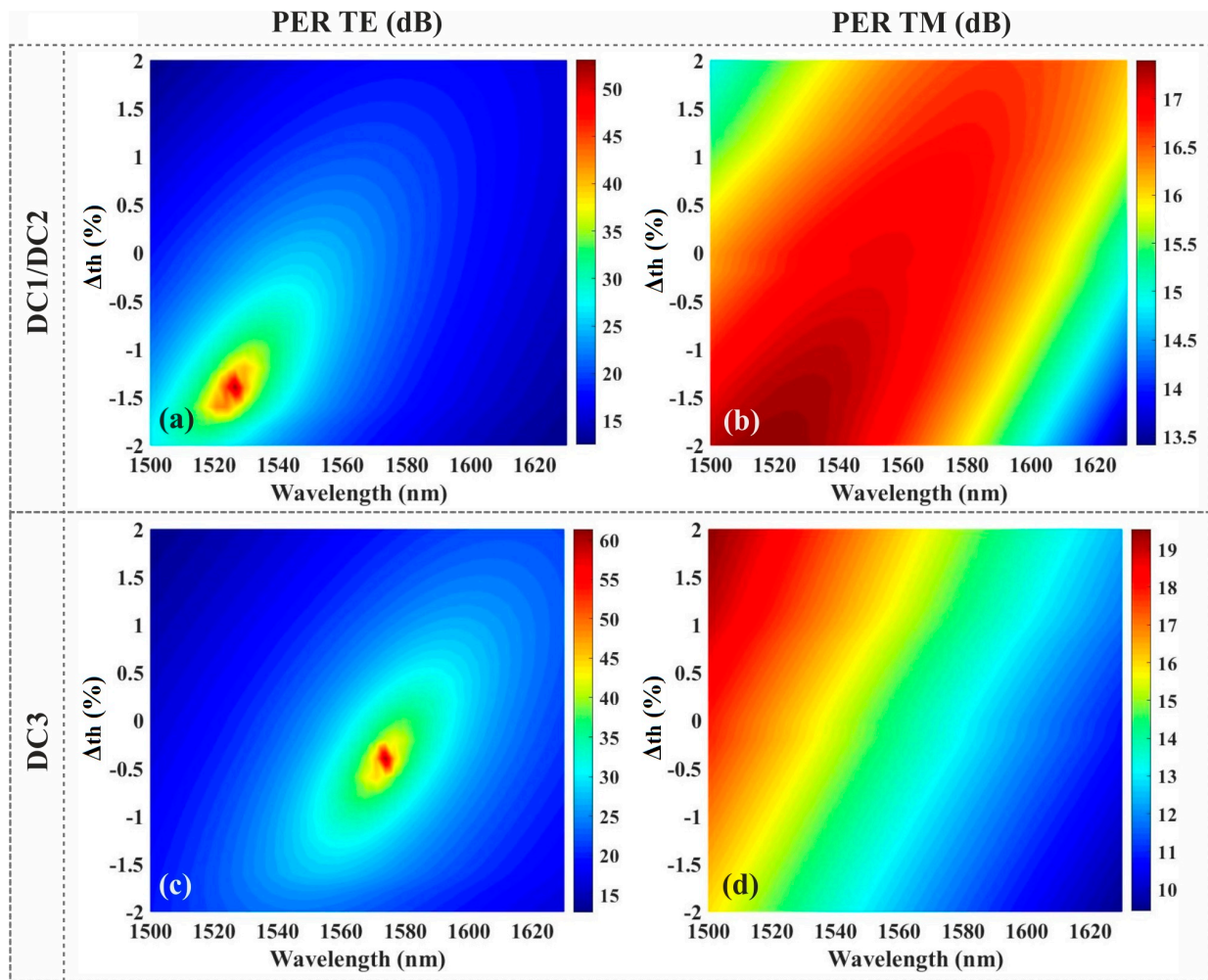


Figure 8. Effect of the variation of thicknesses, Δth , on the TE and TM PER values for (a,b) DC1/DC2 and (c,d) DC3, respectively. Higher and lower Δth values result to a reduction of the minimum PER.

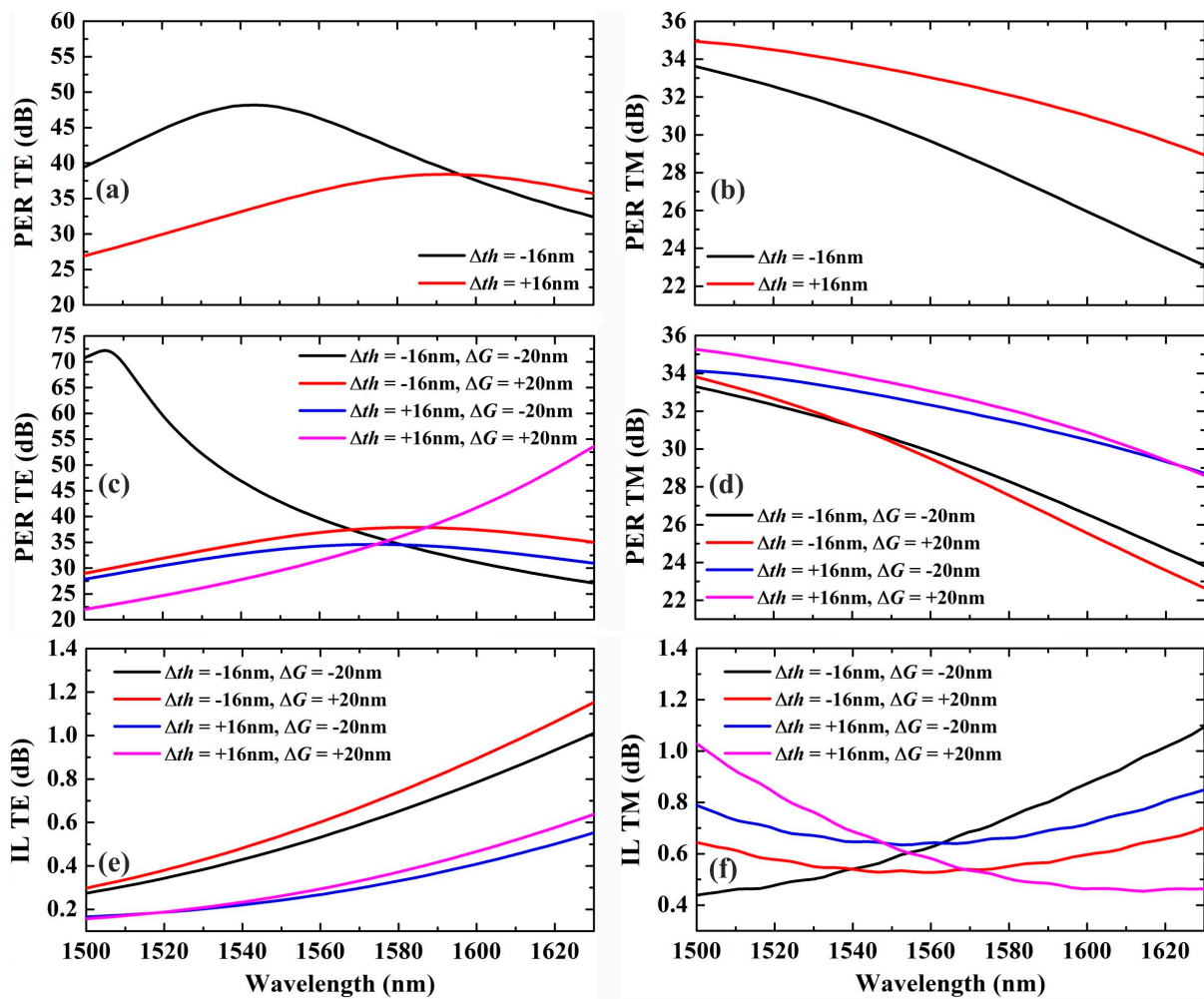


Figure 9. Performance of the PBS cascaded configuration for (a) TE and (b) TM polarization when Δth deviates by ± 16 nm. Corresponding performance curves for (c) TE and (d) TM polarization when $\Delta th = \pm 16$ nm and ΔG deviated by ± 20 nm. IL curves for (e) TE and (f) TM polarization for the four worst-case combinations of Δth and ΔG .

5. Discussion

In this section, the proposed design of this work is compared from every aspect with existing state-of-the-art Si_3N_4 PBSs reported in the literature. Table 2 summarizes the key performance metrics of seven Si_3N_4 PBS designs based on different techniques for direct performance comparison, where “S” refers to the simulated and “E” to the experimental values. The table also includes the number of etching steps required for the fabrication of each design, in order to take into account also the parameter of fabrication complexity. Even though the angled MMI-based PBS of [15] exhibits a slightly lower footprint, it has a minimum PER at least 12.6 dB lower than the one achieved in this work in combination with a 30 nm reduced bandwidth. In addition, the design of [16] exploiting a 2×2 MMI and anodized gratings features a very high PER of >30 dB and low IL, however this comes at the expense of bandwidth that is now only 22 nm, while the footprint is also six times larger. In [10] the operation bandwidth is 95 nm wide at the O-band by cascading phase-controlled DCs, while the minimum PER is 20 dB, but the IL and the footprint are quite higher. In [16] the layout is quite complex, as it is based on handling the first order TM mode from cascaded asymmetric DCs and achieves 80 nm wide operation at the expense of minimum PER, that is only 10 dB. The PBS in [25] is based on cascaded multimode interferometers with very good performance in terms of overall footprint, losses and operational range, but again the minimum PER is only 10 dB for 100 nm range. In [13] the polarization splitting is

relying on a horizontal multi-slot waveguide demonstrating 100 nm bandwidth with more than 20 dB PER within a length of 286 μm . The downside of this design is that the specific cross section of the waveguide must be applied across the whole PIC, if only one etching step is used. Otherwise, two etching steps should be applied for the slot formation. Finally, the design of [17] requires two etching steps for the formation of the three-dimensional vertical directional coupler and achieves more than 16 dB PER over a 30 nm range with very low IL, but the overall footprint is quite large. The last row presents for comparison the key performance metrics of the proposed PBS design that is based on cascaded directional couplers with vertical slots, where superior performance in terms of PER, IL and footprint is exhibited across a very wide 130 nm wavelength span that covers the SCL-band. The separation of the two polarization states follows a similar design strategy exploited on SOI platform in [9], but here significant analysis and optimization in the layout is required, as the basic polarization discrimination mechanism is highly wavelength sensitive and also due to the fact that the effective refractive index of thick Si₃N₄ waveguides is almost identical for the TE and TM polarization. This exceptional performance is coming though at the expense of the higher fabrication complexity required by the two etching depths.

Table 2. Comparison with other PBS designs.

Ref.	Wavelength Range (nm)	Bandwidth (nm)	PER (dB)	IL (dB)	Footprint	Etching Steps	Technique
[14]	1539–1561	22	>30 (S&E)	<1.1 (S&E)	820 × 10 μm^2	1	2×2 MMI and apodized grating
[10]	1260–1355	95	>20 (S&E)	<1.3 (S&E)	240 × 24 μm^2	1	phase-controlled cascaded DCs
[16]	1520–1600	80	>10 (S&E)	<2.1 (S&E)	113 μm long	1	cascaded asymmetric DCs
[25]	1500–1600	100	>10 (S)	<1 (S)	400 × 10 μm^2	1	cascaded MMI
[13]	1500–1600	100	<20 (S)	-	281 μm long	1 or 2	horizontal multi-slot waveguides
[17]	1535–1565	30	>16 (E)	<1 (E)	800 × 20 μm^2	2	3D vertical directional coupler
this work	1500–1630	130	>30.6 (S)	<0.8 (S)	94 × 14 μm^2	2	cascaded DCs with vertical slots

6. Conclusions

In this work, we propose a silicon nitride-based PBS layout that exploits a strip and a vertical slot waveguide, with different thicknesses to discriminate the fundamental modes of the TE and TM polarizations via directional coupling. The device is optimized through extensive FDE and 3D-FDTD electromagnetic simulations, so that the input TM polarized light is directionally coupled from the 470 nm thick strip to the 800 nm thick vertical slot waveguide, while the TE polarized light continues to propagate in the strip waveguide. The proposed PBS design manages to expand the operational window with a high PER for both polarizations, overcoming the inherent wavelength dependence of the directional coupling polarization discrimination mechanism. In the first stage of this analysis, the PBS is optimized for 1550 nm wavelength with maximum IL of 0.18 dB and a minimum PER of 15.4 dB for both polarizations across a 130 nm span at SCL-band. For further optimization of the broadband performance two PBS layouts were identified with variations in the critical parameters of gap G between the slot and strip waveguides and the coupling length L_c in the DC section, aiming for the highest attainable PER at the edges of the targeted window. In this way a cascaded network of two PBSs per polarization port, attains minimum values of 34.3 dB and 30.6 dB for PER_{TE} and PER_{TM} , respectively, a total footprint of 94 × 14 μm^2 and IL lower than 0.8 dB for both polarizations. Finally, a fabrication tolerance analysis was performed taking as worst-case scenarios simultaneous deviations of $\Delta t/h = \pm 16$ nm from optimum thicknesses and $\Delta G = \pm 20$ nm from optimum gap in the DCs. Under these non-optimum conditions, the minimum PER_{TE} and PER_{TM} are calculated above 22 dB, while

the are IL below 1.2 dB in the entire 1500–1630 nm range. These results verify the resilience of the proposed design to provide PER values above the 20 dB benchmark without strict limitations in the fabrication process.

Author Contributions: G.P. wrote the paper and conducted the simulations and analysis, D.K. and D.C. aided in simulations and checked the paper, K.V. supervised. All authors have read and agreed to the published version of the manuscript.

Funding: This research received no external funding.

Institutional Review Board Statement: Not applicable.

Informed Consent Statement: Not applicable.

Data Availability Statement: All data generated during this work can be obtained from the corresponding author upon reasonable request.

Acknowledgments: We highly appreciate the support provided by the European H2020 ICT NEBULA (GA No. 871658) project.

Conflicts of Interest: The authors declare no conflict of interest.

References

1. Siew, S.Y.; Li, B.; Gao, F.; Zheng, H.Y.; Zhang, W.; Guo, P.; Xie, S.W.; Song, A.; Dong, B.; Luo, L.W.; et al. Review of Silicon Photonics Technology and Platform Development. *J. Lightwave Technol.* **2021**, *39*, 4374–4389. [[CrossRef](#)]
2. Chrostowski, L.; Hochberg, M. *Silicon Photonics Design: From Devices to Systems*; Cambridge University Press: Cambridge, UK, 2015.
3. Muñoz, P.; Mico, G.; Bru, L.A.; Pastor, D.; Perez, D.; Domenech, J.D.; Fernandez, J.; Banos, R.; Gargallo, B.; Alemany, R.; et al. Silicon Nitride Photonic Integration Platforms for Visible, Near-Infrared and Mid-Infrared Applications. *Sensors* **2017**, *17*, 2088. [[CrossRef](#)]
4. Asakawa, K.; Sugimoto, Y.; Nakamura, S. Silicon photonics for telecom and data-com applications. *Opto-Electron. Adv.* **2020**, *3*, 200011. [[CrossRef](#)]
5. Heck, M. Highly integrated optical phased arrays: Photonic integrated circuits for optical beam shaping and beam steering. *Nanophotonics* **2017**, *6*, 93–107. [[CrossRef](#)]
6. Morant, M.; Pérez, J.; Llorente, R. Polarization Division Multiplexing of OFDM Radio-over-Fiber Signals in Passive Optical Networks. *Hindawi Adv. Opt. Technol.* **2014**, *2014*, 269524. [[CrossRef](#)]
7. Ivanovich, D.; Powel, S.B.; Gruev, V.; Chamberlain, R.D. Polarization division multiplexing for optical data communications. *SPIE OPTO* **2018**, *15038*, 160–178.
8. Shahwar, D.; Cherchi, M.; Harjanne, M.; Kapulainen, M.; Aalto, T. Polarization splitters for micron-scale silicon photonics. *Proc. SPIE* **2021**, *11691*, 1169104.
9. Tian, Y.; Qiu, J.; Liu, C.; Tian, S.; Huang, Z.; Wu, J. Compact polarization beam splitter with a high extinction ratio over S + C + L band. *Opt. Express* **2019**, *27*, 999–1009. [[CrossRef](#)]
10. Guerber, S.; Ramos, C.A.; Benedikovic, D.; Valdeiglesias, E.D.; Le Roux, X.; Vulliet, N.; Cassan, E.; Morini, D.M.; Baudot, C.; Boeuf, F.; et al. Broadband Polarization Beam Splitter on a Silicon Nitride Platform for O-Band Operation. *IEEE Photonics Technol. Lett.* **2018**, *30*, 2679–2682. [[CrossRef](#)]
11. Gao, S.; Wang, Y.; Wang, K.; Skafidas, E. Low-Loss and Broadband 2×2 Polarization Beam Splitter Based on Silicon Nitride Platform. *IEEE Photonics Technol. Lett.* **2016**, *28*, 1936–1939. [[CrossRef](#)]
12. Jijun, F.; Ryoichi, A. Silicon nitride polarizing beam splitter with potential application for intersubband-transition-based all-optical gate device. *Jpn. J. Appl. Phys.* **2015**, *54*, 04DG08.
13. Fang, Y.; Bao, C.; Wang, Z.; Liu, Y.; Zhang, L.; Huang, H.; Ren, Y.; Pan, Z. Polarization Beam Splitter Based on $\text{Si}_3\text{N}_4/\text{SiO}_2$ Horizontal Slot Waveguides for On-Chip High-Power Applications. *Sensors* **2020**, *20*, 2862. [[CrossRef](#)] [[PubMed](#)]
14. Jhan, J.; Brocj, J.; Veilleux, S.; Dagenais, M. Silicon nitride polarization beam splitter based on polarization-independent MMIs and apodized Bragg gratings. *Opt. Express* **2021**, *29*, 14476–14485.
15. Kudalippallyalil, R.; Murphy, T.E.; Grutter, K. Low-loss and ultra-broadband silicon nitride angled MMI polarization splitter/combiner. *Opt. Express* **2020**, *28*, 34111–34122. [[CrossRef](#)] [[PubMed](#)]
16. Bhandari, B.; Im, C.-S.; Sapkota, O.R.; Lee, S.-S. Highly efficient broadband silicon nitride polarization beam splitter incorporating serially cascaded asymmetric directional couplers. *Opt. Lett.* **2020**, *45*, 5974–5977. [[CrossRef](#)]
17. Feng, J.; Akimoto, R. A Three-Dimensional Silicon Nitride Polarizing Beam Splitter. *IEEE Photonics Technol. Lett.* **2014**, *26*, 706–709. [[CrossRef](#)]

18. Wilmart, Q.; El Dirani, H.; Tyler, N.; Fowler, D.; Malhouitre, S.; Garcia, S.; Casale, M.; Kerdiles, S.; Hassan, K.; Monat, C.; et al. A Versatile Silicon-Silicon Nitride Photonics Platform for Enhanced Functionalities and Applications. *Appl. Sci.* **2019**, *9*, 255. [[CrossRef](#)]
19. El Dirani, H.; Youssef, L.; Petit-Etienne, C.; Kerdiles, S.; Grosse, P.; Monat, C.; Pargon, E.; Sciancalepore, C. Ultralow-loss tightly confining Si₃N₄ waveguides and high-Q microresonators. *Opt. Express* **2019**, *21*, 30726–30740. [[CrossRef](#)]
20. Muñoz, P.; Pastor, D.; Bru, L.A.; Cabanes, G.M.; Benitez, J.; Goodwill, D.; Bernier, E. Scalable Switched Slab Coupler Based Optical Phased Array on Silicon Nitride. *IEEE J. Sel. Top. Quantum Electron.* **2021**, *27*, 1–16.
21. Chatzitheocharis, D.; Ketzaki, D.; Calò, C.; Caillaud, C.; Vyrsokinos, K. Design of Si-rich nitride interposer waveguides for efficient light coupling from InP-based QD-emitters to Si₃N₄ waveguides on a silicon substrate. *Opt. Express* **2020**, *28*, 34219–34236. [[CrossRef](#)]
22. Abouheaf, M.; Gueaieb, W.; Samra, A. Modeling of evanescent-wave coupling between optical dielectric waveguides. *Int. J. Model. Simul.* **2019**, *39*, 38–47. [[CrossRef](#)]
23. Roeloffzen, C.G.H.; Hoekman, M.; Klein, E.J.; Wevers, L.S.; Timens, R.B.; Marchenko, D.; Geskus, D.; Dekker, R.; Alippi, A.; Grootjans, R.; et al. Low-Loss Si₃-N₄ TriPleX Optical Waveguides: Technology and Applications Overview. *IEEE J. Sel. Top. Quantum Electron.* **2018**, *24*, 1–21. [[CrossRef](#)]
24. Chuang, S.L. Waveguide Couplers and Coupled-Mode Theory. In *Physics of Optoelectronic Devices*; Wiley-Interscience: New York, NY, USA, 1995; pp. 283–334.
25. Tosi, M.; Fasciszewski, A.; Rossini, L.A.B.; Costanzo, P.A. Silicon nitride polarisation beam splitters: A review. *IET Optoelectron.* **2019**, *14*, 120–124. [[CrossRef](#)]